

ORTHOTROPIC STRENGTH AND ELASTICITY OF HARDWOODS IN
RELATION TO COMPOSITE MANUFACTURE.
PART II. ORTHOTROPY OF COMPRESSION STRENGTH
AND ELASTICITY

Elemer M. Lang[†]

Assistant Professor

Laszlo Bejo

Graduate Research Assistant
Division of Forestry
West Virginia University
Morgantown, WV 26506-6125

Jozsef Szalai

Professor, Department Head
Department of Technical Mechanics

Zsolt Kovacs

Professor, Director
Institute of Product Development and Technology
University of West Hungary
H-9400 Sopron, Pf.:132
Hungary

and

R. Bruce Anderson

Assistant Professor
Division of Forestry
West Virginia University
Morgantown, WV 26506-6125

(Received April 2001)

ABSTRACT

The effect of grain and annual ring orientation on the compression strength (σ_{uc}) and modulus of elasticity (E_c) of small clear specimens of hardwood species was investigated. The experimental and analytical works explored the orthotropic nature of three North American (quaking aspen, red oak, and yellow-poplar) and two European (true poplar and turkey oak) hardwood species under uniaxial compression. Apparent compression strength and modulus of elasticity were measured at 15° grain and ring angle increments. The three-dimensional Hankinson's formula and another model, based on orthotropic tensor theory, were evaluated for predicting the anatomical direction-dependent properties of the species. Statistical analyses revealed that both models approximate the compression strength and elastic properties reasonably well. Either the analytical or the experimental results can be used for further modeling the orthotropic properties of structural composites.

Keywords: Hardwoods, compression strength and elasticity, orthotropy, modeling.

[†] Member of SWST.

INTRODUCTION

The work presented here is part of an international research program aimed at enlarging the body of knowledge regarding raw material properties of structural composite lumbers. The primary hypothesis of the research is that once the orthotropic engineering and strength properties of the raw materials are assessed, the expected mechanical attributes of a particular composite can be predicted via probabilistic/deterministic models. These models should incorporate the effect of processing parameters on the mechanical properties. However, the investigation of the temperature and/or moisture content effects was beyond the scope of this study. The detailed description of the overall project, justification, and research need have already been discussed previously in a related publication (Lang et al. 2000).

In further exploring the orthotropic nature of different hardwood species that may be potential raw materials for composite manufacture, the orthotropic compression properties were the target of this investigation. The objectives included: generating data for studying the effect of grain and ring orientation on the properties by standard statistical procedures; and validating theoretical models that can predict the anatomical direction-dependent strength and stiffness of the examined species under compression.

This paper provides a literature review of research works on orthotropic compression properties and discusses possible theoretical approaches. In addition, it describes the experimental and analytical works performed, along with conclusions and further modeling possibilities.

BACKGROUND

Orthotropy of the mechanical properties of wood has been an area of interest in wood science for a long time. Generally uniaxial strength and elastic properties were investigated, both because of their ease of assessment

and importance in practical applications. Much research effort was concentrated in this area. However, the majority of these works focused on the effect of either grain or ring angle, separately.

The most well-known model to describe the effect of sloping grain on compression properties is the Hankinson's formula (Hankinson 1921). Radcliffe (1965) investigated the accuracy of the equation, comparing its predictions to theoretical values of modulus of elasticity (E_c) that were derived from the relationships of orthotropic elasticity. He showed that Hankinson's solution is quite accurate in the longitudinal-radial (LR) plane, while in the longitudinal-tangential (LT) plane around 25° grain inclination, it may underestimate the E value by 30%. Other researchers also verified the validity of this model (Goodman and Bodig 1972; Bodig and Jayne 1982). Kollmann and Côté (1968) suggested some modifications to the original formula. Cowin (1979) gave a good overview of these developments, and concluded that the valid formula should be the one Hankinson originally proposed. Some published research works claimed that another version, the Osgood formula, approximates the effect of sloping grain better than the Hankinson's equation (Kim 1986; Bindzi and Samson 1995). The Osgood formula, which is also empirical, is given as follows:

$$n = \frac{pq}{q + (p - q)\sin^2\varphi(\sin^2\varphi + a \cos^2\varphi)} \quad (1)$$

where n , p , and q are the compression properties at grain angles φ , 0°, and 90°, respectively. Constant a is a species-specific coefficient that should be determined experimentally. However, no extensive validation of this model was reported in the literature (Kim 1986).

Transverse compression has received much attention, too. Bodig (1965), Kunesh (1968), and Bendsten et al. (1978) provided more in-depth analysis of the question. Ethington et al. (1996) incorporated variation of ring orienta-

tion in their work, and concluded that it had significant effect on the compression strength perpendicular to the grain.

The exact determination of the strength perpendicular to the grain is practically impossible because of the difficulties of ultimate stress determination. The ASTM D 143-83 (ASTM 1996a) standard requires that the test shall be discontinued after 0.1-inch (2.5-mm) cross-head-displacement. This procedure was developed to evaluate the reaction force supporting capacity of solid wood joists. Consequently, there is no standard testing method that regulates the exploration of orthotropy in compression. However, there are several theories for predicting the failure envelope of solid wood and/or wood-based composites. Usually these approaches are based either four or four plus two-dimensional tensor analyses like the Tsai-Wu strength criterion (Tsai and Wu 1971). This approach was developed two decades ago for homogeneous, orthotropic materials such as glass or carbon fiber and epoxy composites. The fiber direction in these synthetic composites is better controlled, and the materials are transversely isotropic (i.e., identical strength and elastic properties in any direction perpendicular to the fiber). Thus, such analyses can be successfully used in exploring the strength orthotropy of relatively homogeneous materials as demonstrated through an analysis of paperboard by Suhling et al. (1985).

Although wood is usually modeled as an orthotropic material, in reality it is cylindrically orthotropic. The inherent natural variability of wood, coupled with the ambiguous definition of failure stresses, generates several difficulties in application of advanced failure theories. Furthermore, the compression strength determination of cross-grained wood blocks always depends on the size, shape, manufacturing precision (parallelism), and support conditions of the specimen.

Consider an ideal, cross-grained specimen for compression strength assessment in a global coordinate system as shown on Fig. 1 where the anatomical directions (L , R , and T) are

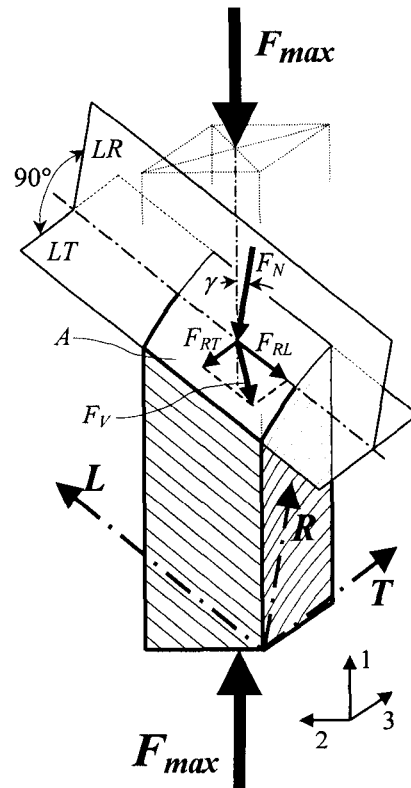


FIG. 1. Internal force condition of an oblique specimen under compression.

marked, as well. In an arbitrarily selected LT principal anatomical plane of the specimen, the compression force (F_{max}) can be broken into a normal (F_N) and in-plane (F_V) components. The area (A) of this inclined sectional surface can be approximated using trigonometric identities. F_V can be represented as a resultant of F_{RL} and F_{RT} that induce parallel-to-the-grain shear stress at 0° ring angle and rolling shear, respectively. If the ratio of F_V to the sectional area of the specimen (F_V/A) in the LT plane exceeds the shear strength ($\tau_{\vartheta\Theta}$), the specimen will fail in shear under compression. The subscripts ϑ and Θ are the angles between F_V and the direction of the fibers, and between the sheared and LT planes, respectively. For this particular case, $\Theta = 0$. Because several species demonstrated relatively low degree of shear orthotropy concerning the ring orientation, one can realize that shear fail-

ure is possible in any plane between LT and LR, if the induced shear stresses are large enough. In fact, off axis compression specimens were used to evaluate the shear strength of Finnish pine by Ylinen (1963) in the *LT* and *LR* planes. The relationship between shear and normal stresses for grain inclination range of $12^\circ < \varphi < 32^\circ$ was given as follows:

$$\tau_{max} = 1/2 \sigma_{max} \sin 2\varphi \quad (2)$$

One should note that this shear failure stress is biased by a compression stress (σ_q) normal to the plane of failure:

$$\sigma_q = \sigma_{max} \sin^2 \varphi \quad (3)$$

where $\sigma_{max} = \sigma_1$ is the ultimate compression stress in the global coordinate system and φ is the grain angle.

Experimental results of Ylinen (1963) showed that there is a consistent shear strength difference at the studied grain angles between the *LR* and *LT* planes. It indicates some interactions between grain and ring orientations. The ambiguous failure modes, coupled with the inherent natural variability of wood, allow the exploration of apparent strength only for particularly defined specimens. The size, the slenderness ratio of the specimen, and the end conditions, along with the existence or lack of lateral supports, may affect the measured compression strength values. Furthermore, the determination of E in compression may be also biased by some of these conditions, and the induced shear strain may affect the measured normal strain.

The complexity of the failure phenomena and the above-discussed problems make the predictions difficult and sometimes unreliable. However, some approaches that incorporate both the ring and grain angle variations can predict the orthotropic properties with reasonable accuracy. Such methods, that were verified and used during this research, are briefly discussed next.

MODELING THE ORTHOTROPY OF COMPRESSION STRENGTH AND E_c

Selection criteria for models that can predict both E_c and compression strength were sim-

licity, minimum input requirements, and validity at any grain (φ) and ring angle (θ) combination. While the simplicity is not a vital problem because of the advances in computer science, models that needed all nine independent elastic constants as inputs were not considered. Therefore, two procedures, a theoretical and an empirical one, were selected.

Strength/stiffness tensor theory

Szalai (1994) provided an approach for calculating the normal strength of orthotropic materials in any direction. The equation can be derived from the Ashkenazi's strength tensor (Ashkenazi 1978) by transforming the first element of the tensor. After eliminating the zero components, the equation takes the following form:

$$\begin{aligned} \frac{1}{\hat{\sigma}_{\varphi\theta}} &= \frac{1}{\sigma_L} \cos^4 \varphi + \frac{1}{\sigma_R} \sin^4 \varphi \sin^4 \theta \\ &+ \frac{1}{\sigma_T} \sin^4 \varphi \cos^4 \theta \\ &+ \left(\frac{4}{\sigma_{RT}^{L45^\circ}} - \frac{1}{\sigma_R} - \frac{1}{\sigma_T} \right) \sin^4 \varphi \sin^2 \theta \cos^2 \theta \\ &+ \left(\frac{4}{\sigma_{LT}^{R45^\circ}} - \frac{1}{\sigma_R} - \frac{1}{\sigma_T} \right) \cos^2 \varphi \sin^2 \varphi \cos^2 \theta \\ &+ \left(\frac{4}{\sigma_{LR}^{T45^\circ}} - \frac{1}{\sigma_L} - \frac{1}{\sigma_R} \right) \cos^2 \varphi \sin^2 \varphi \sin^2 \theta \end{aligned} \quad (4)$$

where: $\hat{\sigma}_{\varphi\theta}$ = predicted compression strength at grain angle φ and ring angle θ ;

σ_i = compression strength in the principal anatomical directions ($i = L, R, T$);

$\sigma_{RT}^{L45^\circ}$ = compression strength at $\varphi = 90^\circ$; $\theta = 45^\circ$;

$\sigma_{LT}^{R45^\circ}$ = compression strength at $\varphi = 45^\circ$; $\theta = 0^\circ$;

$\sigma_{LR}^{T45^\circ}$ = compression strength at $\varphi = 45^\circ$; $\theta = 90^\circ$.

The six strength values listed in Eq. (4)

should be determined experimentally. Note that by replacing the strength with the appropriate $E_{\varphi\theta}$ values, the evaluation of elastic orthotropy can be performed. The appendix contains the derivation of this tensorial approach from the compliance matrix and from the Ashkenazi's strength tensor for E values determination and strength evaluation, respectively.

Three-dimensional Hankinson's formula

Bodig and Jayne (1982) based their approach partly on the Hankinson formula, and on the observed compression strength pattern in the RT plane. According to the authors, the strength variation pattern in this plane consists of a linear and a sinusoidal component:

$$\sigma_{90^\circ;\theta} = \left[\sigma_T + \frac{\theta}{\pi/2} (\sigma_R - \sigma_T) \right] + \left[K(-\sin 2\theta) \frac{\sigma_R + \sigma_T}{2} \right] \quad (5)$$

where: $\sigma_{90^\circ;\theta}$ = the predicted compression strength at 90° grain angle and ring angle θ ;

K = empirical constant (0.2 for hardwoods).

Other notations are as in Eq. (1).

After calculating this value for a certain ring angle, strength or MOE properties belonging to any grain angle at the given ring angle level can be obtained by substituting this value and σ_L into the Hankinson formula:

$$\hat{\sigma}_{\varphi\theta} = \frac{\sigma_L \sigma_{90^\circ;\theta}}{\sigma_L \sin^2 \varphi + \sigma_{90^\circ;\theta} \cos^2 \varphi} \quad (6)$$

This empirical approach lacks the firm theoretical basis of the orthotropic tensor theory. However, this method requires only three experimentally determined data points in the principal anatomical directions, and the calculation is no more difficult than in the case of the previous formula. Equations (4) and (6) were first validated and then were used to predict the orthotropic compression properties of the examined species as follows.

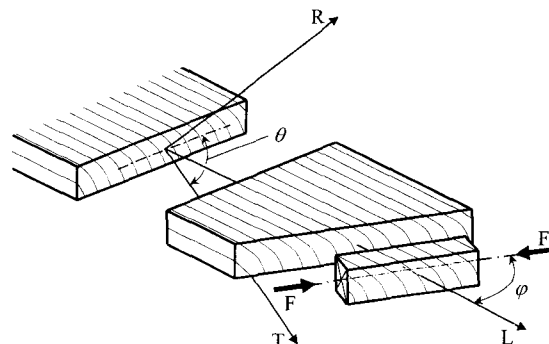


FIG. 2. Specimen manufacturing practice and the interpretation of φ and θ .

MATERIALS AND METHODS

Standard ASTM specimens (ASTM D 143-83, 1996a secondary method) were prepared from quaking aspen (*Populus tremuloides*), red oak (*Quercus rubra*), and yellow-poplar (*Liriodendron tulipifera*) species. Trees were harvested from the West Virginia University (WVU) forest and sawn into lumber. Specimens from the European species including turkey oak (*Quercus cerris*) and true poplar (*Populus x. Euramericana cv. Pannonia*) were manufactured at West Hungarian University using locally available commercial lumber. The final dimensions ($25 \times 25 \times 100$ mm) were set after conditioning the blank materials to approximately 12% moisture content (MC) in a controlled environment (i.e., 21°C and 65% RH).

Ring and grain angles of the specimens varied between 0° and 90° with 15° increments. Ring angle is not defined at 0° grain orientation, and its effect was disregarded at 15° grain angle. The experimental design, therefore, contained only one set of 10 specimens at both 0° and 15° . Figure 2 shows the specimen manufacturing practice and the interpretation of grain (φ) and ring (θ) angles. Moisture content and specific gravity (SG) determination were done using representative samples of specimens ($n = 10$). The evaluation of these physical properties followed the specifications of standards ASTM D 4442-84 and ASTM D 2395-83 (ASTM 1996, c, b).

During the validation of the models for both strength and stiffness, the North American species were used. Approximately 160 specimens of each species provided 4 to 10 replications for each variable (φ/θ) combination. Testing apparatus included an MTS servo-hydraulic universal machine, equipped with a 10 kN \pm 1 N load cell. Cross-head movement was under displacement control. Compression load application occurred through a self-aligning block placed on top of the specimen. A computerized data acquisition system collected the load and displacement data in real time. Screw-mounted knife-edge pieces held in place the clip-on extensometers that provided displacement data throughout the test, over a gauge length of 41 mm. Two gauges measured the deformations at the opposite, side-grained surfaces of the specimens. The obtained pairs of displacement values were averaged, and the corresponding load-displacement data were converted into stress-strain diagrams for further analyses. Figure 3 demonstrates the experimental assembly. Other parameters of the procedure, including the speed of testing, agreed with the specifications of ASTM D 143-83 standard (ASTM 1996a). Load application continued until failure or until the densification plateau of horizontally grained ($\varphi \approx 90^\circ$) specimens was explicitly reached. The failure type of each specimen was visually assessed and recorded.

Compression E values of the European species were tested at the laboratory of WVU using the above-described techniques. Before testing, the specimens were reconditioned, and the parallelism of the surfaces was checked. Only the combinations required for model inputs were evaluated by testing 15 replications per factor/level group.

The Hungarian partners measured the strength values on a screw-driven, universal testing machine. Because of machine constraints, the speed of testing was 0.5 mm/min. This is slightly higher than that of ASTM requirement. Other parameters including specimen size and conditioning were the same as at WVU. For possible probability modeling of

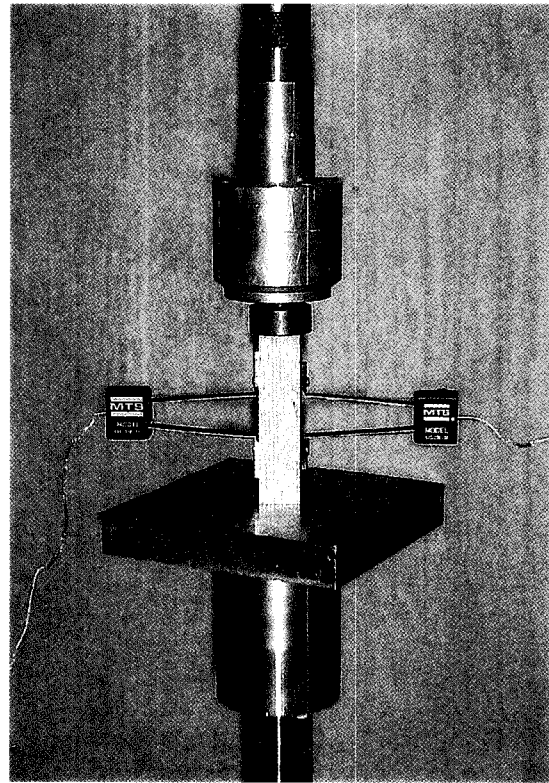


FIG. 3. Compression force application and the two-sided strain measurement.

the strength properties, the number of replications were set to 300 during this evaluation. Discussion of the obtained probability density functions and the objectives of the mentioned modeling are beyond the scope of this paper.

The applied statistical methods included the calculation of descriptive statistics and analyses of variances (ANOVA) procedures. We established the validity of the models by curve fitting. Concerns over justification of the usage of these statistical procedures and the detailed description of the r^2 calculation in three-dimensional curve fitting have already been presented elsewhere (Lang et al. 2000).

RESULTS AND DISCUSSION

Tables 1, 2, and 3 contain the summary statistics of the measured properties. These results represent all the experimental data. No outliers were discarded. In general, the prop-

TABLE 1. Summary and basic statistics of the experimentally determined compression *E* values

Aspen																						
Mean and standard deviation values are in GPa																						
Ring Orientation (θ°)																						
0 15 30 45 60 75 90																						
Grain angle (φ°)	Compression <i>E</i>																					
	<i>n</i> ^a	\bar{x} ^b	<i>s</i> ^c	<i>n</i>	\bar{x}	<i>s</i>																
0	—	—	—	—	—	—	—	—	—	10	10.74	1.71	—	—	—	—	—	—	—	—	—	—
15	—	—	—	—	—	—	—	—	—	10	6.10	0.83	—	—	—	—	—	—	—	—	—	—
30	5	1.60	0.25	4	1.70	0.29	4	1.91	0.12	6	1.96	0.59	4	2.31	0.26	4	3.37	1.18	6	2.45	0.44	—
45	6	0.72	0.10	4	0.99	0.15	4	0.63	0.06	6	0.53	0.11	4	1.45	0.89	4	0.90	0.11	6	2.10	0.46	—
60	6	0.46	0.27	3	0.42	0.05	4	0.34	0.18	6	0.44	0.09	4	0.43	0.03	4	0.90	0.26	6	0.98	0.19	—
75	6	0.24	0.05	4	0.18	0.02	4	0.21	0.02	6	0.24	0.03	4	0.42	0.14	4	0.78	0.14	6	0.37	0.05	—
90	6	0.26	0.03	4	0.24	0.07	3	0.33	0.03	5	0.36	0.03	4	0.36	0.04	4	0.54	0.05	5	0.82	0.26	—
Oak																						
Mean and standard deviation values are in GPa																						
Ring Orientation (θ°)																						
0 15 30 45 60 75 90																						
Grain angle (φ°)	Compression <i>E</i>																					
	<i>n</i> ^a	\bar{x} ^b	<i>s</i> ^c	<i>n</i>	\bar{x}	<i>s</i>																
0	—	—	—	—	—	—	—	—	—	11	14.40	2.16	—	—	—	—	—	—	—	—	—	—
15	—	—	—	—	—	—	—	—	—	10	8.43	2.20	—	—	—	—	—	—	—	—	—	—
30	6	3.03	0.33	4	3.44	0.29	4	2.58	0.29	6	2.10	0.86	4	4.46	0.94	4	3.78	0.29	6	3.85	0.21	—
45	6	2.42	0.20	4	2.03	0.27	4	1.59	0.22	6	1.59	0.10	4	2.19	0.34	4	2.08	0.29	6	2.41	0.29	—
60	6	1.62	0.23	4	1.49	0.18	4	1.24	0.07	6	1.44	0.18	4	1.68	0.13	4	1.31	0.12	6	1.81	0.27	—
75	6	1.04	0.10	4	1.13	0.07	4	1.00	0.07	6	1.11	0.05	4	1.72	0.33	4	0.97	0.15	6	1.84	0.22	—
90	6	1.04	0.14	3	0.93	0.19	4	0.97	0.07	6	0.92	0.06	4	1.32	0.15	4	0.97	0.07	6	1.61	0.29	—
Yellow-poplar																						
Mean and standard deviation values are in GPa																						
Ring Orientation (θ°)																						
0 15 30 45 60 75 90																						
Grain angle (φ°)	Compression <i>E</i>																					
	<i>n</i> ^a	\bar{x} ^b	<i>s</i> ^c	<i>n</i>	\bar{x}	<i>s</i>																
0	—	—	—	—	—	—	—	—	—	10	10.26	1.47	—	—	—	—	—	—	—	—	—	—
15	—	—	—	—	—	—	—	—	—	10	7.15	1.33	—	—	—	—	—	—	—	—	—	—
30	6	3.25	0.84	4	2.72	0.20	4	3.26	0.35	6	2.55	0.15	4	3.20	0.33	4	3.21	0.11	6	2.39	0.22	—
45	6	1.46	0.11	4	1.64	0.67	4	1.49	0.13	6	1.45	0.16	4	1.64	0.07	4	1.01	0.06	6	1.18	0.35	—
60	6	0.82	0.09	4	0.80	0.08	4	0.98	0.07	6	0.79	0.08	4	1.13	0.07	4	0.66	0.07	6	0.97	0.13	—
75	6	0.55	0.24	4	0.65	0.07	4	0.73	0.04	6	0.51	0.05	4	0.60	0.06	4	0.49	0.03	6	0.53	0.14	—
90	6	0.37	0.04	4	0.73	0.07	4	0.66	0.04	6	0.40	0.02	4	0.73	0.04	4	0.43	0.05	6	0.74	0.11	—

^a Sample size. ^b Mean value. ^c Standard deviation.

TABLE 2. Summary and basic statistics of the experimentally determined compression strength values.

Aspen																					
Mean and standard deviation values are in MPa																					
Ring Orientation (θ°)																					
0		15			30			45			60			75			90				
Grain angle (φ°)	Compression E																				
	n ^a	\bar{x} ^b	s ^c	n	\bar{x}	s	n	\bar{x}	s	n	\bar{x}	s	n	\bar{x}	s	n	\bar{x}	s	n	\bar{x}	s
0	—	—	—	—	—	—	—	—	—	10	36.23	1.14	—	—	—	—	—	—	—	—	—
15	—	—	—	—	—	—	—	—	—	10	28.55	2.64	—	—	—	—	—	—	—	—	—
30	6	10.54	1.99	4	11.33	0.33	4	11.05	0.44	6	12.27	1.21	4	13.25	1.17	4	10.54	4.94	6	12.55	0.71
45	6	6.52	0.52	4	8.15	1.12	4	6.09	0.60	6	5.13	0.39	4	6.61	0.78	4	6.16	0.19	6	8.35	0.89
60	6	3.63	0.19	4	4.24	0.19	4	4.05	0.54	6	3.88	0.37	4	3.77	0.02	4	5.81	0.08	6	5.08	1.24
75	6	3.18	0.30	4	2.88	0.12	4	3.01	0.13	6	2.62	0.10	4	3.31	0.60	4	4.97	0.14	6	3.12	0.10
90	6	3.07	0.13	4	3.07	0.18	4	3.38	0.13	6	3.44	0.09	4	3.70	0.24	4	4.14	0.10	5	4.28	0.13
Oak																					
Mean and standard deviation values are in MPa																					
Ring Orientation (θ°)																					
0		15			30			45			60			75			90				
Grain angle (φ°)	Compression E																				
	n ^a	\bar{x} ^b	s ^c	n	\bar{x}	s	n	\bar{x}	s	n	\bar{x}	s	n	\bar{x}	s	n	\bar{x}	s	n	\bar{x}	s
0	—	—	—	—	—	—	—	—	—	9	49.72	2.75	—	—	—	—	—	—	—	—	—
15	—	—	—	—	—	—	—	—	—	10	41.76	2.67	—	—	—	—	—	—	—	—	—
30	6	28.31	1.58	4	33.23	1.95	4	26.81	1.74	6	18.17	5.08	4	27.74	2.00	4	25.72	1.62	6	24.25	1.11
45	6	22.13	0.34	4	23.24	1.94	4	17.18	0.69	6	13.14	0.14	4	16.96	2.77	4	14.42	0.31	6	17.01	0.58
60	6	13.91	0.54	4	16.06	0.75	4	12.99	0.99	6	13.62	1.70	4	10.85	0.64	4	10.23	0.05	6	13.07	0.60
75	6	11.25	0.21	4	13.30	0.41	4	9.81	0.30	6	11.03	0.20	4	9.19	0.52	4	8.22	0.13	6	11.29	0.35
90	6	10.17	0.21	3	11.63	0.42	4	9.35	0.24	6	9.77	0.49	4	9.36	0.17	4	7.65	0.29	6	11.32	0.43
Yellow-poplar																					
Mean and standard deviation values are in MPa																					
Ring Orientation (θ°)																					
0		15			30			45			60			75			90				
Grain angle (φ°)	Compression E																				
	n ^a	\bar{x} ^b	s ^c	n	\bar{x}	s	n	\bar{x}	s	n	\bar{x}	s	n	\bar{x}	s	n	\bar{x}	s	n	\bar{x}	s
0	—	—	—	—	—	—	—	—	—	10	35.47	2.52	—	—	—	—	—	—	—	—	—
15	—	—	—	—	—	—	—	—	—	10	33.35	3.74	—	—	—	—	—	—	—	—	—
30	6	20.84	1.44	4	19.03	0.40	4	21.37	0.87	6	19.55	0.97	4	16.70	1.20	4	15.56	1.07	6	17.33	0.41
45	6	13.08	0.68	4	12.89	4.32	4	12.80	0.42	6	13.77	0.88	4	11.46	0.20	4	9.07	0.18	6	9.22	1.76
60	6	8.19	0.09	4	7.97	0.11	4	8.40	0.29	6	7.81	0.29	4	8.07	0.18	4	6.66	0.24	6	8.12	0.22
75	6	6.71	0.19	4	6.50	0.06	4	6.80	0.14	6	5.46	0.37	4	6.35	0.21	4	5.60	0.14	6	5.35	0.28
90	6	4.38	0.15	4	5.99	0.14	4	6.31	0.08	6	4.42	0.08	4	6.40	0.23	4	5.16	0.10	6	7.13	0.16

^a Sample size. ^b Mean value. ^c Standard deviation.

TABLE 3. Summary and basic statistics of the experimentally determined compression strength and E values of European hardwood species.

Grain angle (φ°)	Ring angle (θ°)	True poplar						Turkey oak					
		Compression E (GPa)			Compression strength (MPa)			Compression E (GPa)			Compression strength (MPa)		
		n ^a	\bar{x} ^b	s ^c	n	\bar{x}	s	n	\bar{x}	s	n	\bar{x}	s
0	—	11	10.35	1.31	300	34.45	2.69	15	11.03	1.57	300	51.97	6.82
45	0	15	0.63	0.07	300	6.32	1.00	14	1.69	0.12	216	21.36	3.11
45	90	15	1.36	0.12	300	8.72	1.20	15	2.66	0.27	298	22.92	3.26
90	0	15	0.25	0.01	300	3.04	0.31	15	0.93	0.11	300	10.02	0.95
90	45	15	0.25	0.02	297	3.00	0.38	14	0.98	0.06	300	10.94	1.21
90	90	15	0.71	0.05	300	4.37	0.65	15	1.97	0.23	300	14.67	1.75

^a Sample size.^b Mean value.^c Standard deviation.

erties of similar species are comparable, except for turkey oak, which had somewhat lower E_c values around 0 degree grain orientation compared to the values of red oak. The high degree of orthotropy was evident for all species for both strength and stiffness as a response to grain angle changes. However, the effect of ring orientation was not so clear. It does appear that the changing ring orientation at grain angles $< 45^\circ$ causes strength and stiffness to decrease. At more sloping grain angles, the increasing ring angle tends to improve the compression properties slightly. For all species and for both properties, two-way ANOVA procedures revealed the statistically significant effect of both ring and grain angle at 95% confidence level. Furthermore, the interactions between these factors were also significant. Table 4 contains a typical outcome of the ANOVA procedures. Figure 4a demonstrates the stress-strain behavior of compression-parallel-to-the-grain specimens by the North American species. In Fig. 4b the characteristics of compression

perpendicular to the grain at 15° ring orientation can be seen. The long horizontal part of the diagram is the result of subsequent cellular collapse of earlywood followed by latewood layers. The stabilized stresses in this region were considered as strength values if the specimen did not fail in shear prior to densification. Figure 4c demonstrates the intense compression strength decrease as a function of grain orientation.

Predictions of the compression properties

The mean values were used to create anisotropy diagrams in a three-dimensional polar coordinate system as shown on Figs. 5a and 6a for E_c of red oak and strength of yellow-poplar, respectively. The seven values, indicated at 15° grain angle, all correspond to the one average value of ten replications that were measured at this level at random ring orientations. The intermediate mesh data were interpolated using the inverse distance method (SPSS Inc. 1997).

In the next step, the two models discussed were evaluated for the accuracy of their estimation. The required model inputs, specified earlier, were the average measured strength and E_c values. The model-generated property data were plotted as orthotropy diagrams for visual evaluation. Figures 5 and 6 provide examples for E_c and strength prediction of red oak and yellow-poplar, respectively. In these figures, diagrams marked as *b* represent the

TABLE 4. Analysis of Variance table for the compression strength of aspen.

Source	df	Sum of squares	Mean square	P value
Angle variation	34	1,774	52.2	< 0.001
Grain angle	4	1,660	415.1	< 0.001
Ring angle	6	39	6.4	< 0.001
Grain \times Ring	24	75	3.1	< 0.001
Random error	134	133	0.989	
Total	168	1,906		

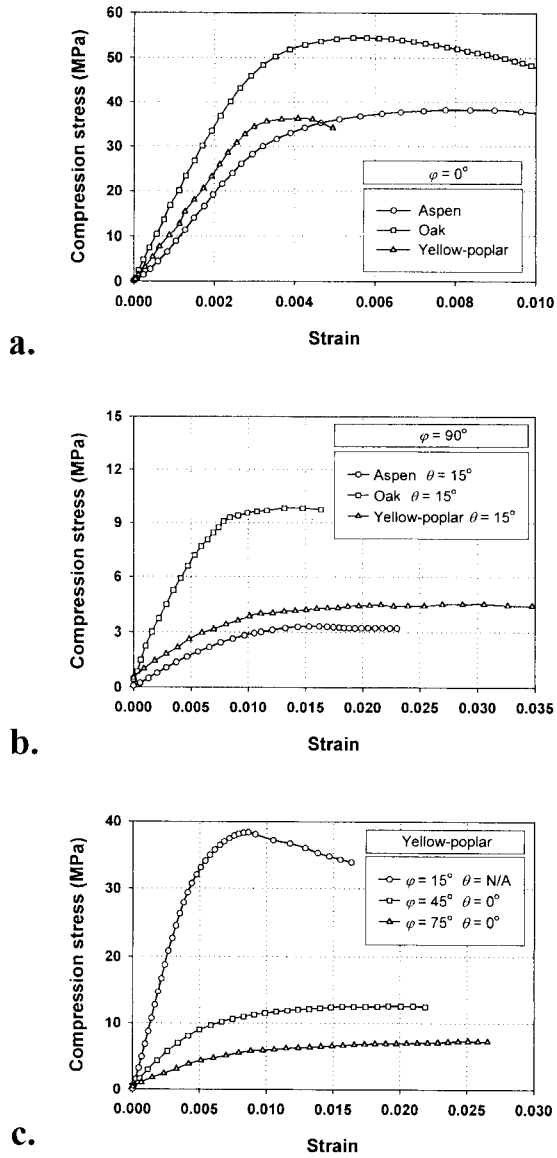


FIG. 4. Typical stress-strain diagrams. a. Parallel-to-the-grain compression; b. Perpendicular-to-the-grain compression; c. The effect of grain orientation.

predicted values derived from tensor analysis using Eq. (4). Diagrams marked as *c* show the predictions of 3D Hankinson's formula. These diagrams clearly confirm the individual and interaction effect of φ and θ on the strength and *E* values in compression.

Statistical comparisons of experimental and predicted properties by curve fitting confirmed

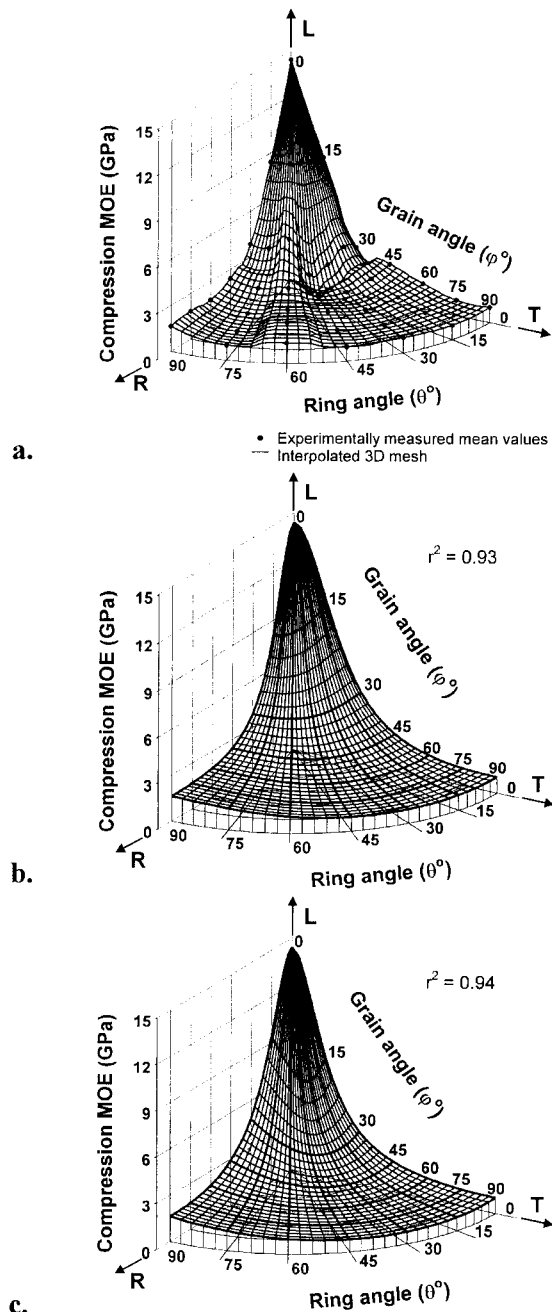


FIG. 5. Orthotropy diagrams of compression modulus of elasticity of oak. a. Experimental and interpolated values; b. Prediction of the tensorial model; c. Prediction of the 3D Hankinson's formula.

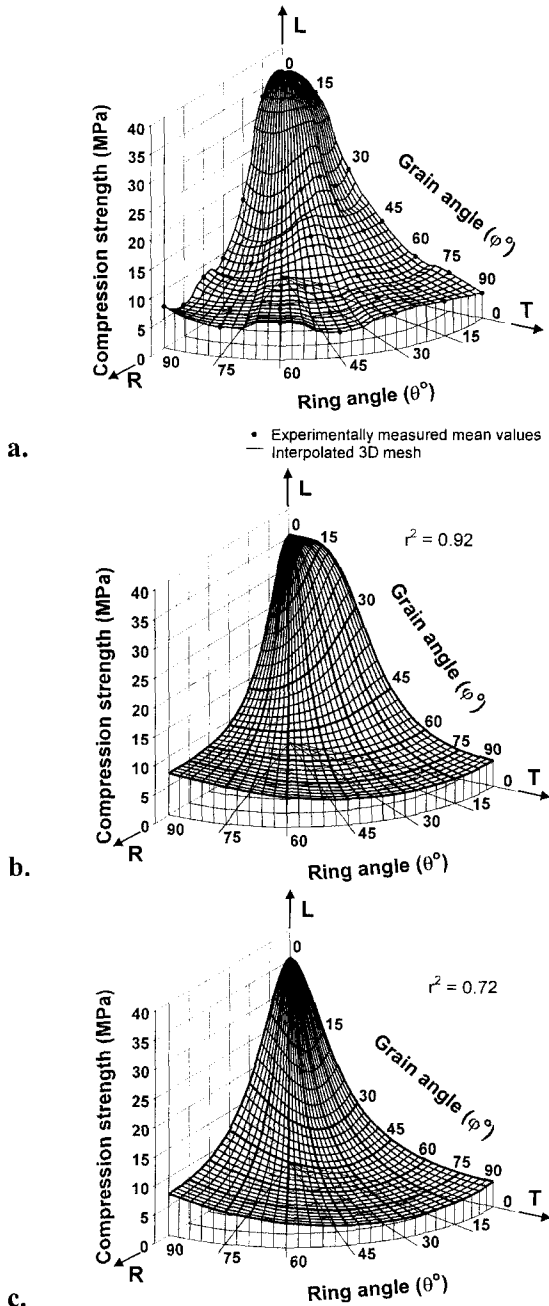


FIG. 6. Orthotropy diagrams of compression strength yellow-poplar. a. Experimental and interpolated values; b. Prediction of the tensorial model; c. Prediction of the 3D Hankinson's formula.

the applicability of these models. Table 5 contains the results of the analyses by species and model types. For aspen and red oak, in the cases of compression strength and E_c , both models demonstrated excellent agreement ($r^2 > 0.9$). For yellow-poplar, however, the prediction quality of the Hankinson's formula decreased, although the r^2 values remained on acceptable levels for both strength and stiffness. The phenomena may be explained by the sensitivity of the Hankinson's equation to small grain angle variations. This is particularly manifested during strength predictions where the effect of small grain deviation on the experimentally measured strength is less significant.

Failure mode analysis

In modeling the compression strength, a failure criterion developed by Ashkenazi (1978) was assumed (Eq. 4). Nahas (1986) provided detailed evaluation of this criterion along with others. Although the criterion includes the interaction effect, the basic assumption of it is that the failure is independent from the deformation. Consequently, it can not provide information about the type of failure.

During the compression strength determination, several types of failure were observed. Figure 7 shows the most characteristic failure modes, where specimen *a* demonstrates a typical compression failure. Specimens *b* and *c* failed as a combination of cellular collapse and shear as indicated by the horizontal dislocation of certain parts of the blocks. Clear shear failures in the *LR* and *LT* planes are represented by specimens *d* and *e*, respectively. Most of the perpendicular-to-the-grain specimens ($\phi = 90^\circ$) did not fail at all, due to the unique densification characteristic of solid wood. For safety reasons, tests were stopped as soon as the stress level explicitly stabilized in the plateau region (Fig. 4b).

The complexity of failure mode prediction was addressed briefly in an earlier section. In further elaboration of this issue, Fig. 8 demonstrates the likelihood of shear failure as-

TABLE 5. Coefficients of determination (r^2) provided by the two prediction models for compression strength and E_c .

Species	Orthotropic tensor theory		3-D Hankinson formula	
	Compression strength	Compression E	Compression strength	Compression E
Aspen	0.93	0.94	0.91	0.91
Oak	0.93	0.93	0.93	0.94
Yellow-poplar	0.92	0.93	0.72	0.83

assessment in the cases of two particular angle combinations under compression stress. First, consider a red oak specimen with $\varphi = 45^\circ$ and $\theta = 15^\circ$ grain and ring orientations under $\sigma_u = 23.24$ MPa compression stress in the global coordinate system. Note that σ_u is the average compression strength of oak for the particular φ/θ combination (Table 2). In Fig. 8, the mesh represents the principal shear strength of oak in planes parallel to the grain (Lang et al. 2000). Possible combinations of ϑ and Θ are defined by the interdependence of the grain orientation of F_V and the rotation angle of the parallel-to-the-grain sheared plane (see Fig. 1). The principal shear strength values at these angle combinations form the solid line within the strength surface, which denotes the possible shearing scenarios of the specimen. This line can be considered as the critical shear stress contour of the examined φ/θ compression specimen. The corresponding shear stresses, computed from $\sigma_u = 23.24$ MPa and the in-

clined sectional areas (A), are represented by the symbols and drop-lines. Solid symbols mark the compression-induced shear stresses that exceed the estimated shear strength, while the empty symbols mark the stresses that are below the strength values. Theoretically, the specimens should have failed in shear; however, because of the natural variability of wood and the presence of normal stresses in the sheared places, usually a combined failure was observed as shown in Fig. 7c.

The second example demonstrates that compression may induce shear failure in a horizontally grained specimen too. For specimens

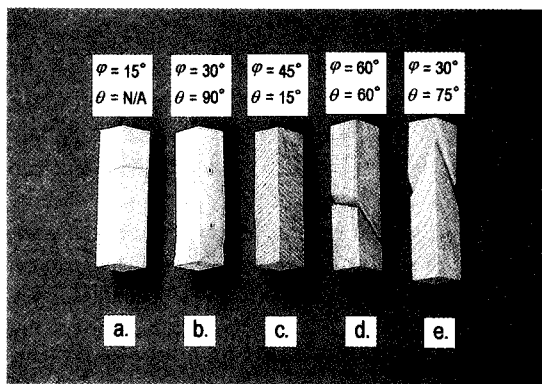


FIG. 7. Typical failure modes. a. Compression failure; b. Combined shear and compression failure; c. Combined shear and compression failure; d. Shear failure in the LR plane; e. Shear failure in the LT plane.

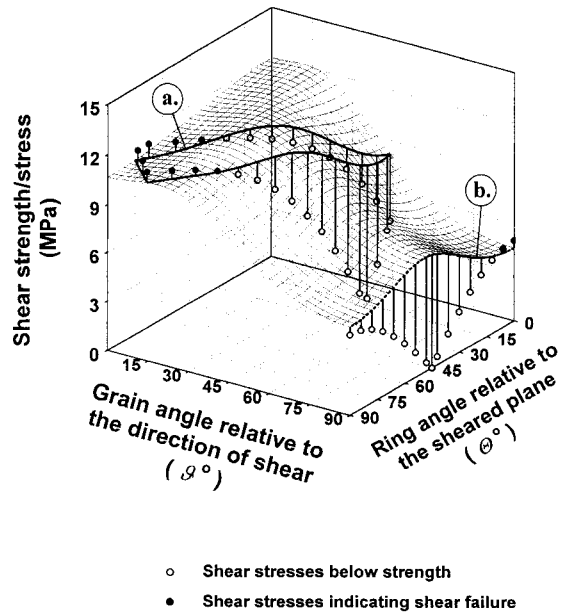


FIG. 8. Likelihood of shear failure in red oak compression specimens. a. Critical shear stress contour of specimen $\varphi = 45^\circ$, $\theta = 15^\circ$; $\sigma_u = 23.24$ MPa; b. Critical shear stress contour of specimen $\varphi = 90^\circ$, $\theta = 45^\circ$; $\sigma_u = 9.77$ MPa.

with $\varphi = 90^\circ$ and $\theta = 45^\circ$, the average strength (σ_u) was 9.77 MPa. The critical shear stress contour, in this case, reduces to a single line (dotted in Fig. 8) along the lower edge of the shear strength surface because the direction of shear is always perpendicular to the direction of grain for this specimen configuration. The calculated stresses exceed the strength values in the range of $15^\circ > \Theta > 0^\circ$. This domain represents inclined planes around 45° relative to the length of the specimen in which shear failure may occur. At $\Theta = 45^\circ$ the shear stress is zero because no shear can be induced along the vertical or horizontal planes in the global coordinate system by compression. Unfortunately, the practical application of such analysis is limited, because of the uncertainties in shear strength determination and variations in growth characteristics of natural wood. One might consider that more advanced failure theories like the Tsai-Wu or von Mises criteria may provide better assessment of compression strength. However, the parameter determination of these criteria involves the same uncertainties due to inherent variability of wood. Some of the delicate experimental techniques used for assessing properties of synthetic composites are not viable for solid wood. Nevertheless, it may be stated that there is no single failure theory that can be applied to all species and wood-based composites and to all loading conditions.

SUMMARY AND CONCLUSIONS

The analytical and experimental investigations of the orthotropic nature of compression strength and modulus of elasticity were presented. Apparent strength and stiffness values were obtained by testing of systematically manufactured specimens with varying grain and ring angles. Statistical analyses revealed the significant individual and combined effects of grain and ring orientations on the compression properties for five species. Furthermore, two models, based on tensor analysis and the Hankinson's equation, were validated experimentally. Both models proved to be reason-

ably accurate in predicting the strength and stiffness of small, clear compression specimens in any oblique anatomical direction. Failure mode analyses highlighted the difficulties of the shear, compression, or combined type failure prediction.

The experimental results obtained and the validated models can be used for modeling and/or assessing the compression properties of structural composites. In these products, the alignment of the wooden constituents can be deterministic, random, or both. In modeling, a strength or stiffness can be assigned to these constituents according to their orientation. However, further research is needed to explore the effect of processing parameters on the material properties. It may include the investigation of peeling/stranding process and the evaluation of time, temperature, and moisture content effects on the constituent's properties.

It was pointed out that the evaluation of compression properties might be significantly affected by several factors including species, size, and testing scenarios. The authors wish to draw the reader's attention to the fact that the findings of this research have limited universal values. Care should be taken in extrapolation of the results for wood species and testing conditions other than specified in this paper.

ACKNOWLEDGMENTS

This research is partially financed by the McIntire-Stennis Forestry Research Act, project No.: 978 at West Virginia University and the Hungarian National Science Foundation (OTKA) project No.: T 025985. The international cooperation has been made possible through the North Atlantic Treaty Organization (NATO), Cooperative Research Grant, CRG.LG 973967. The financial supports are gratefully acknowledged. This manuscript is published with the approval of the Director of the West Virginia Agricultural and Forestry Experiment Station as Scientific Article No. 2799.

REFERENCES

- AMERICAN SOCIETY FOR TESTING AND MATERIALS. 1996a. Standard methods of testing small clear specimens of timber, ASTM D 143-83. ASTM, West Conshohocken, PA.
- . 1996b. Standard test methods for specific gravity of wood and wood-base materials. ASTM D 2395-83. ASTM, West Conshohocken, PA.
- . 1996c. Standard test methods for direct moisture content measurement of wood and wood-base materials. ASTM D 4442-83. ASTM, West Conshohocken, PA.
- ASHKENAZI, E. K. 1978. Anizotropia drevesinu i drevesinuh materialov. (Anisotropy of wood and wood-based materials.) Lesnaja Pramushlemnosty, Moscow, USSR. (in Russian).
- BENDSTEN, B. A., J. H. HASKELL, AND W. L. GALLIGAN. 1978. Characterizing the stress-compression relationship of wood in compression perpendicular to grain. *Wood Sci.* 10(3):111-121.
- BINDZI, I., AND M. SAMSON. 1995. New formula for influence of spiral grain on bending stiffness of wood beams. *ASCE, J. Struct. Eng.*, 121(11):1541-1546.
- BODIG, J. 1965. The effect of anatomy on the initial stress-strain relationship in transverse compression. *Forest Prod. J.* 15(4):197-202.
- , AND B. A. JAYNE. 1982. *Mechanics of wooden and wood composites.* Van Nostrand Reinhold Co., New York, NY.
- COWIN, S. C. 1979. On the strength anisotropy of bone and wood. *J. Appl. Mech.* 46(12):832-838.
- ETHINGTON, R. L., V. ESKELSEN, AND R. GUPTA. 1996. Relationship between compression strength perpendicular to grain and ring orientation. *Forest Prod. J.* 46(1):84-86.
- HANKINSON, R. L. 1921. Investigation of crushing strength of spruce at varying angles of grain. Air Service Information Circular No. 259, U.S. Air Service.
- GOODMAN, J. R., AND J. BODIG. 1972. Orthotropic strength of wood in compression. *Wood Sci.* 4(2):83-94.
- KIM, K.Y. 1986. A note on Hankinson formula. *Wood Fiber Sci.* 18(2):345-348.
- KOLLMAN, F. P. P., AND W. A. CÔTÉ JR. 1968. *Principles of wood science and technology, I.* Springer-Verlag, New York, NY.
- KUNESH, R. H. 1968. Strength and elastic properties of wood in transverse compression. *Forest Prod. J.* 18(1):65-72.
- LANG, E. M., L. BEJO, J. SZALAI, AND Z. KOVACS. 2000. Orthotropic strength and elasticity of hardwoods in relation to composite manufacture. Part I. Orthotropy of shear strength. *Wood Fiber Sci.* 32(4):502-519.
- NAHAS, M. N. 1986. Survey of failure and post failure theories of laminated fiber reinforced composites. *J. Composite Technol. Res.* 8(4):138-153.
- RADCLIFFE, B. M. 1965. A theoretical evaluation of Hankinson formula for modulus of elasticity of wood at an angle to the grain. *Quart. Bull. Michigan Agr. Exp. Station.* 48(2):286-295.
- SPSS INC. 1997. *SigmaPlot® 4.0 for Windows.* SPSS Inc., Chicago, IL.
- SUHLING, J. C., R. E. ROWLANDS, M. W. JOHNSON, AND D. E. GUNDERSON. 1985. Tensorial strength analysis of paperboard. *Exp. Mech.* 42:75-84.
- SZALAI, J. 1994. Anisotropic strength and elasticity of wood and wood based composites. Private ed. Sopron, Hungary. (in Hungarian).
- TSAI, W. S., AND E. M. WU. 1971. A general theory of strength for anisotropic materials. *J. Composite Mater.* 5(1):58-80.
- YLINEN, A. 1963. A comparative study of different types of shear tests of wood. Paper presented on the Fifth Conference of Wood Technology. U.S. Forest Products Laboratory, September 16-27, Madison, WI.

APPENDIX

Derivation of the orthotropic tensor model

The compliance matrix of solid wood, as an orthotropic material, in terms of its elastic constants, is given as follows:

$$\begin{bmatrix} \frac{1}{E_L} & -\frac{\nu_{RL}}{E_R} & -\frac{\nu_{TL}}{E_T} & 0 & 0 & 0 \\ -\frac{\nu_{LR}}{E_T} & \frac{1}{E_R} & -\frac{\nu_{TR}}{E_T} & 0 & 0 & 0 \\ -\frac{\nu_{LT}}{E_L} & -\frac{\nu_{RT}}{E_R} & \frac{1}{E_T} & 0 & 0 & 0 \\ 0 & 0 & 0 & \frac{1}{G_{RT}} & 0 & 0 \\ 0 & 0 & 0 & 0 & \frac{1}{G_{TL}} & 0 \\ 0 & 0 & 0 & 0 & 0 & \frac{1}{G_{LR}} \end{bmatrix} \quad (\text{A.1})$$

where: E_i = modulus of elasticity of wood in the i anatomical direction;
 G_{ij} = shear modulus in the main anatomical planes, where i is the direction normal to the sheared plane and j is the direction of the applied load;
 ν_{ij} = Poisson ratio (i is the direction of passive strain and j is the direction of the applied load.)
 $i, j = L, R, \text{ and } T$

Considering the orthotropic symmetry and the relationships between the elastic parameters, it can be shown that:

$$-\frac{\nu_{ij}}{E_j} = \frac{1}{2} \left(\frac{4}{E_{ij}^{45^\circ}} - \frac{1}{E_i} - \frac{1}{E_j} - \frac{1}{G_{ij}} \right) \quad (\text{A.2})$$

where: $E_{ij}^{45^\circ}$ = The modulus of elasticity of wood in the ij plane, at a 45° direction between i and j .

Substituting the above relationship (A.2) into A.1, the elements of the compliance matrix can be defined in the following form:

$$\begin{bmatrix} \frac{1}{E_L} & \frac{1}{2} \left(\frac{4}{E_{LR}^{745^\circ}} - \frac{1}{E_L} - \frac{1}{E_R} - \frac{1}{G_{RL}} \right) & \frac{1}{2} \left(\frac{4}{E_{LT}^{845^\circ}} - \frac{1}{E_L} - \frac{1}{E_T} - \frac{1}{G_{TL}} \right) & 0 & 0 & 0 \\ \frac{1}{2} \left(\frac{4}{E_{LR}^{745^\circ}} - \frac{1}{E_L} - \frac{1}{E_R} - \frac{1}{G_{RL}} \right) & \frac{1}{E_R} & \frac{1}{2} \left(\frac{4}{E_{RT}^{L45^\circ}} - \frac{1}{E_R} - \frac{1}{E_T} - \frac{1}{G_{RT}} \right) & 0 & 0 & 0 \\ \frac{1}{2} \left(\frac{4}{E_{LT}^{845^\circ}} - \frac{1}{E_L} - \frac{1}{E_T} - \frac{1}{G_{TL}} \right) & \frac{1}{2} \left(\frac{4}{E_{RT}^{L45^\circ}} - \frac{1}{E_R} - \frac{1}{E_T} - \frac{1}{G_{RT}} \right) & \frac{1}{E_T} & 0 & 0 & 0 \\ 0 & 0 & 0 & \frac{1}{G_{RT}} & 0 & 0 \\ 0 & 0 & 0 & 0 & \frac{1}{G_{TL}} & 0 \\ 0 & 0 & 0 & 0 & 0 & \frac{1}{G_{RL}} \end{bmatrix} \quad (A.3)$$

The above matrix is a simplified two-dimensional representation of a four-dimensional tensor. According to the transformation rules of a four-dimensional tensor, when the coordinate system is rotated around its origin, an element of the new tensor can be calculated by the formula:

$$t_{i'j'k'l'} = \sum t_{ijkl} \beta_{i'}^i \beta_{j'}^j \beta_{k'}^k \beta_{l'}^l \quad (A.4)$$

where: $t_{i'j'k'l'}$ = an element of the new tensor ($i', j', k', l' = x, y, z$)
 t_{ijkl} = an element of the original tensor ($i, j, k, l = L, R, T$)
 $\beta_{i'}^i$ = the length of the orthogonal projection of a unit vector in the direction of the i 'th coordinate axis in the new coordinate system, on the i th axis in the old coordinate system

Figure A.1 shows three examples, where $i' = x$ and $i = L, R, T$.

Let the new coordinate system be chosen so that its x axis is aligned with the compression load (F). In this case, transforming the first element of the tensor ($t_{LLLL} = 1/E_L$), will provide the reciprocal of the E_c in the x direction, the direction designated by φ and θ as defined in Fig. A.1 (where: $t_{xxxx} = 1/E_x = 1/E_{\varphi\theta}$).

The transformation requires the determination of $\beta_{x'}^L$, $\beta_{x'}^R$, and $\beta_{x'}^T$ only. Figure A.1 shows the calculation of these coordinates. Applying the transformation rule (Eq. A.4) to the first element of the matrix yields the following formula for the calculation of the E_c in a chosen direction:

$$\begin{aligned} \frac{1}{E_{\varphi\theta}} &= \frac{1}{E_L} \cos^4 \varphi + \frac{1}{E_R} \sin^4 \varphi \sin^2 \theta + \frac{1}{E_T} \sin^4 \varphi \cos^2 \theta \\ &+ \left(\frac{4}{E_{RT}^{L45^\circ}} - \frac{1}{E_R} - \frac{1}{E_T} \right) \sin^4 \varphi \sin^2 \theta \cos^2 \theta \\ &+ \left(\frac{4}{E_{LT}^{845^\circ}} - \frac{1}{E_L} - \frac{1}{E_T} \right) \cos^2 \varphi \sin^2 \varphi \cos^2 \theta \\ &+ \left(\frac{4}{E_{LR}^{745^\circ}} - \frac{1}{E_L} - \frac{1}{E_R} \right) \cos^2 \varphi \sin^2 \varphi \sin^2 \theta \end{aligned} \quad (A.5)$$

where $\hat{E}_{\varphi\theta}$ = predicted compression MOE at grain angle φ and ring angle θ ;
 E_i = compression E in the principal anatomical directions ($i = L, R, T$);
 $E_{RT}^{L45^\circ}$ = compression E at $\varphi = 90^\circ$; $\theta = 45^\circ$;
 $E_{LT}^{845^\circ}$ = compression E at $\varphi = 45^\circ$; $\theta = 0^\circ$;
 $E_{LR}^{745^\circ}$ = compression E at $\varphi = 45^\circ$; $\theta = 90^\circ$.

Note that this two-step transformation eliminated the Poisson's ratios and shear moduli, and only six experimentally predetermined E_c values are needed to predict the modulus of elasticity in any oblique direction.

The derivation of the tensorial formula for compression strength is based on similar transformations. Ashkenazi (1978) hypothesized that the strength of an orthotropic material can be described similarly to its elastic properties. Accordingly, the fourth order strength tensor of a solid wood block can be represented by the following matrix:

$$\begin{bmatrix}
 \frac{1}{\sigma_L} & \frac{1}{2} \left(\frac{4}{\sigma_{LR}^{745^\circ}} - \frac{1}{\sigma_L} - \frac{1}{\sigma_R} - \frac{1}{\tau_{RL}} \right) & \frac{1}{2} \left(\frac{4}{\sigma_{LT}^{R45^\circ}} - \frac{1}{\sigma_L} - \frac{1}{\sigma_T} - \frac{1}{\tau_{TL}} \right) & 0 & 0 & 0 \\
 \frac{1}{2} \left(\frac{4}{\sigma_{LR}^{745^\circ}} - \frac{1}{\sigma_L} - \frac{1}{\sigma_R} - \frac{1}{\tau_{RL}} \right) & \frac{1}{\sigma_R} & \frac{1}{2} \left(\frac{4}{\sigma_{RT}^{L45^\circ}} - \frac{1}{\sigma_R} - \frac{1}{\sigma_T} - \frac{1}{\tau_{RT}} \right) & 0 & 0 & 0 \\
 \frac{1}{2} \left(\frac{4}{\sigma_{LT}^{R45^\circ}} - \frac{1}{\sigma_L} - \frac{1}{\sigma_T} - \frac{1}{\tau_{TL}} \right) & \frac{1}{2} \left(\frac{4}{\sigma_{RT}^{L45^\circ}} - \frac{1}{\sigma_R} - \frac{1}{\sigma_T} - \frac{1}{\tau_{RT}} \right) & \frac{1}{\sigma_T} & 0 & 0 & 0 \\
 0 & 0 & 0 & \frac{1}{\tau_{RT}} & 0 & 0 \\
 0 & 0 & 0 & 0 & \frac{1}{\tau_{TL}} & 0 \\
 0 & 0 & 0 & 0 & 0 & \frac{1}{\tau_{RL}}
 \end{bmatrix} \quad (A.6)$$

Transforming the first element of the above matrix the same way as that of the compliance matrix provides the equation:

$$\begin{aligned}
 \frac{1}{\hat{\sigma}_{\varphi\theta}} &= \frac{1}{\sigma_L} \cos^4 \varphi + \frac{1}{\sigma_R} \sin^4 \varphi \sin^4 \theta + \frac{1}{\sigma_T} \sin^4 \varphi \cos^4 \theta \\
 &+ \left(\frac{4}{\sigma_{RT}^{L45^\circ}} - \frac{1}{\sigma_R} - \frac{1}{\sigma_T} \right) \sin^4 \varphi \sin^2 \theta \cos^2 \theta \\
 &+ \left(\frac{4}{\sigma_{LT}^{R45^\circ}} - \frac{1}{\sigma_L} - \frac{1}{\sigma_T} \right) \cos^2 \varphi \sin^2 \theta \cos^2 \theta \\
 &+ \left(\frac{4}{\sigma_{LR}^{745^\circ}} - \frac{1}{\sigma_L} - \frac{1}{\sigma_R} \right) \cos^2 \varphi \sin^2 \theta \sin^2 \theta \quad (A.7)
 \end{aligned}$$

where: $\hat{\sigma}_{\varphi\theta}$ = predicted compression strength at grain angle φ and ring angle θ ;
 σ_i = compression strength in the principal anatomical directions ($i = L, R, T$);
 $\sigma_{RT}^{L45^\circ}$ = compression strength at $\varphi = 90^\circ$; $\theta = 45^\circ$;
 $\sigma_{LT}^{R45^\circ}$ = compression strength at $\varphi = 45^\circ$; $\theta = 0^\circ$;
 $\sigma_{LR}^{745^\circ}$ = compression strength at $\varphi = 45^\circ$; $\theta = 90^\circ$.

Similarly, the advantage of this approach is that only six predetermined properties are needed for predicting the strength values in the entire domain. These principal ultimate stresses can be easily assessed. The disadvantage

of this method is that only uniaxial strengths can be evaluated (i.e., tension or compression). Furthermore, the model can predict the apparent strength with reasonable accuracy; however, it can not indicate the failure mode.

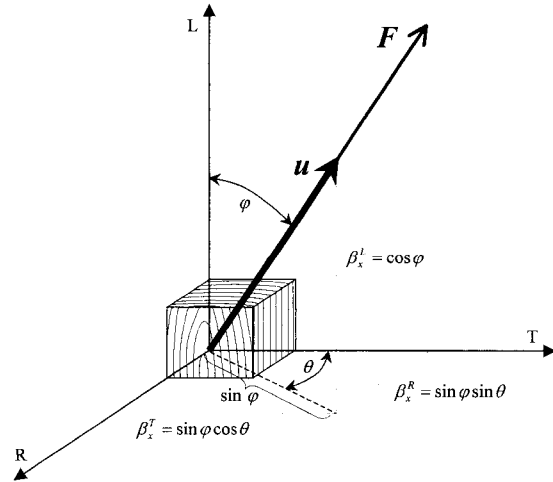


FIG. A.1. Interpretation of grain angle (φ) and ring orientation (θ) relative to the applied compression load and the definition of β_x^L , β_x^R , and β_x^T . F direction of the applied load; u unit vector in the direction of applied load.